

# Chemistry of Lipid Membranes from Models to Living Systems: A Perspective of Hydration, Surface Potential, Curvature, Confinement and Heterogeneity

Halil I. Okur,<sup>1</sup> Orly B. Tarun, and Sylvie Roke\*<sup>1</sup>

Laboratory for Fundamental BioPhotonics (LBP), Institute of Bioengineering (IBI) and Institute of Materials Science (IMX), School of Engineering (STI) and Lausanne Center for Ultrafast Science (LACUS), École Polytechnique Fédérale de Lausanne (EPFL), CH-1015 Lausanne, Switzerland

**ABSTRACT:** Lipid membranes provide diverse and essential functions in our cells relating to transport, energy harvesting and signaling. This variety of functions is controlled by the molecular architecture, such as the presence of hydrating water, specific chemical compounds and microscopic structures, such as the local membrane curvature, as well as macroscopic properties, such as the fluidity of the membrane. To understand the chemistry of membranes, ideally one needs access to multiple length scales simultaneously, using probes that are noninvasive, label-free and membrane-interface specific. This dream is generally pursued by following either a top-down approach, introducing labels to real cell membranes or by following a bottom-up approach with well-controlled but simplified membrane monolayer or supported membrane models. This Perspective offers an alternative path that ultimately envisions bringing together both approaches. By using intermediate nano-, micro- and macroscale free-floating membrane systems in combination with novel nonlinear optical methods, one can advance the understanding of realistic membranes on a more fundamental level. Here, we describe recent advances in understanding membrane molecular structure, hydration, electrostatics and the effect of variable length scale, curvature and confinement for 3D nano- and microscale membrane systems such as lipid droplets and liposomes. We also describe an approach to image membrane hydration and membrane potentials in real time and space together with an application to neuroscience. In doing so, we consider the emerging role of interfacial transient structural heterogeneities that are apparent in both model membranes as well as in whole cells.

## INTRODUCTION

A cell membrane functions as a barrier of permeability that compartmentalizes cells. At this place, the cell performs crucial functions such as receiving signals (plasma membrane),<sup>1,2</sup> energy conversion (mitochondrial membrane)<sup>3,4</sup> and metabolic conversion (adiposome organelle interface).<sup>5–8</sup> As such, the majority of chemicals and drugs in the body interact with lipid membranes and their constituents. Lipid membranes are complex and composed of a diverse mixture of lipids that provide a semifluid environment for peptides and proteins.<sup>9–12</sup>

The membrane electrostatic potential,<sup>13–17</sup> chemical compounds,<sup>18–22</sup> spatiotemporal distribution of molecules,<sup>23,24</sup> the size and curvature of the membrane<sup>25–27</sup> and presence or absence of (transient) domains<sup>28,29</sup> play key roles in the diverse chemistry of membranes and the above-mentioned processes. On an even more fundamental level, all membrane constituents are surrounded by water molecules. Without this hydrating water, the above-mentioned constituents are not able to self-assemble into a bilayer membrane.

Mapping membrane structure including hydration and its role in the dynamics of charge, the interactions with proteins, as well as membrane-modifying mechanisms in situ in real-time and space and in living systems is thus of prime importance to understand the chemistry of life. This is an ideal that should be realized in the future. It is also a formidable challenge, and one that has not been achieved so far. The most challenging aspect about obtaining interfacial molecular-level information as well as membrane hydration is that the probing methods should be label-free, nonperturbative, interface specific, able to discern different chemical structures, and spatially and temporally resolved on multiple length scales, and capable to measure in turbid media. Such complex technology does not yet exist. Therefore, to understand membrane functions, two distinct approaches are generally followed, represented in Figure 1: a top-down and a bottom-up approach. The first one uses real cells and applies (mostly optical) tools that allow accessing certain aspects of cellular functioning. Most commonly, one uses probes such as dye molecules or nanoparticles that have been engineered to address certain cellular processes and measures the fate of these probes.<sup>24,30,31</sup> Due to the abundance of probes and their bright emission,<sup>12,24,28,30,31</sup> it has become possible to achieve single molecule microscopy of membranes in living systems,<sup>32</sup> and to obtain subsecond images of dynamic membrane processes in them.<sup>33</sup> However, membrane interface specificity is not inherently present in the methods. Since the chemistry of living systems involves a delicate balance, this approach does not result in molecular-level information and inherently cannot capture the role of water. More specifically, the resonant enhancement of the probe response overwhelms the intrinsically weak linear or nonlinear optical contribution of the water response. The second approach uses simplified model systems that mimic certain aspects of membranes, such as lipid monolayers (LMs)<sup>34–38</sup> and supported lipid bilayers

Received: March 14, 2019

Published: July 19, 2019

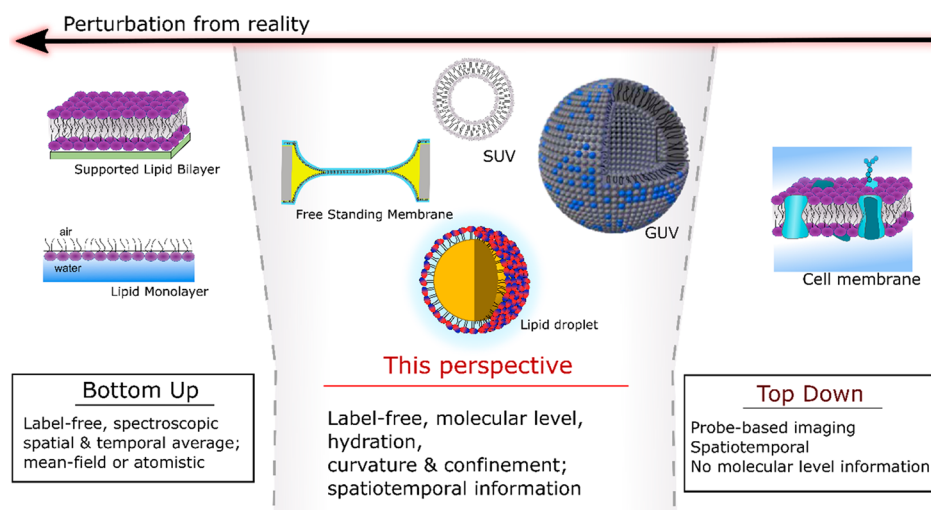


**Figure 1.** Model membrane systems with bottom-up and top-down approaches used to understand the complex biochemistry and physics of membrane interfaces. In this Perspective, we describe an approach to achieve label-free, molecular-level, hydration and spatiotemporal probing of membrane interfaces of 3D nanoscale and microscale free-floating membranes. This approach represents an intermediate step toward obtaining full molecular to macroscopic understanding of the chemistry of membranes. Part of the figure is adapted from ref 59 with permission from the American Chemical Society.

(SLBs).<sup>39–41</sup> Using these systems in combination with interface-sensitive spectroscopic tools, it has become possible to learn a great deal about the chemical complexity of LMs and SLBs,<sup>35,37,42–48</sup> the role of electrostatics,<sup>49–52</sup> and water.<sup>34,45,46,53–55</sup> Aside from these two extremes, other more realistic model systems are known, such as nano- and microscale lipid droplets (LDs)<sup>53,56–58</sup> and liposomes (or small and large unilamellar vesicles, SUVs and LUVs, respectively),<sup>13,59,60</sup> as well as giant unilamellar vesicles (GUVs) and freestanding lipid membranes (FLMs)<sup>15,23</sup> that are all fully embedded in an aqueous phase. These model systems are more realistic and molecular level and hydration information is emerging, owing to recent technological developments as further discussed in this Perspective. In the far future, one might expect or dream that the top-down and bottom-up approach of Figure 1 come together, and that it will be possible to measure spatially resolved real-time molecular-level information on each molecule at the membrane interfaces of living cells. A far better understanding of membrane chemistry, as well as a much better handle on the development of new drugs and biomedical technology will be achieved. This dream can potentially be reached by using the intermediate free-floating membrane systems (LDs, SUV-GUVs and FLMs) as stepping stones, highlighted in the middle section of Figure 1.

In this Perspective, we describe several recent advances made during the last five years on the path toward this goal. We briefly introduce technology that enables one to obtain molecular-level interfacial information about structure and hydration of more realistic free floating nano-, micro- and macroscale membrane model systems in aqueous solution. This information is obtained from molecular-specific nonlinear light scattering spectroscopy and spatiotemporal wide-field second harmonic imaging experiments. Recent experiments on diverse length scales illustrate the importance of curvature, confinement, length-scale and heterogeneity in space and time.

This Perspective starts with a description of the state of the art, summarizing the bottom-up approach to obtain interface specific membrane and hydration structure using LMs and

SLBs. In the next section ([Nano- and Microscale Membrane Model Systems](#)), we describe the possibility of detecting molecular structural information and hydration structure of lipid droplets and liposomes in solution. Examples of recent studies in which the surface and hydration structure of LDs and liposomes that have a different composition is altered are discussed. This is followed by a discussion of how the angle resolved nonlinear light scattering data can be converted into water orientational and membrane potential information ([Electrostatic Membrane Potential](#)). The findings in terms of structure and electrostatics are then compared to knowledge obtained from experiments on LMs and SLBs, giving rise to emerging insights into the effects of length scales, curvature and confinement ([Length Scale and Curvature](#)). To further understand the role of length scales we discuss an approach to obtain real-time spatially resolved molecular-structural information on membrane water ([Spatiotemporal Imaging of Membrane Water](#)), as well as the first surprising results: Membrane water imaging experiments reveal spatiotemporal fluctuation in the hydration of freestanding membranes, confirming that membrane chemistry cannot be understood as a mean-field phenomenon that assumes a spatially and temporally uniform energy landscape. Instead, membrane chemistry is steered by fluctuations in time and space of the structure and energy landscape that depends on effects such as the length scale of the system, confinement and curvature. Before discussing the implications of all of these in a final outlook section, we demonstrate an application of water imaging to probe the spatiotemporal membrane potential fluctuations in activated living neurons ([Membrane Potential Imaging in Living Neurons](#)). Here, spatiotemporal heterogeneities are also observed in living membrane systems.

**Molecular-Level Information on Membranes: State of the Art.** To obtain detailed membrane specific information, lipids,<sup>35,55,61–64</sup> proteins<sup>65,66</sup> and nanoparticles<sup>67</sup> have been investigated on LMs at the planar extended air/water interface, as well as in SLBs<sup>42,44,68</sup> using sum frequency generation (SFG) and second harmonic generation (SHG), the techniques that are primarily discussed in this Perspective.

SHG and SFG are second-order nonlinear optical spectroscopic probes that are inherently sensitive to interfaces due to symmetry induced vanishing response from bulk media. SFG is a combination of infrared (IR) and Raman spectroscopy and provides interfacial vibrational spectra, while SHG is primarily used to probe electronic structure. A more detailed description of these techniques in relation to scattering and imaging can be found in the next section. Membrane hydration was probed on SLBs<sup>49</sup> and on LMs at the planar extended air/water interface.<sup>54,55,69</sup> These studies show that depending on the lipid (and substrate) used, membrane/monolayer water differs in structure. The ionic speciation within the electric double layer and at the interface influences the electrostatic energy landscape and is thus a critical membrane structure determining factor. In addition (Hofmeister) alkali and alkaline-earth metal cations and transition metal cations are known for a wide range of specific ion effects, ranging from signaling by means of cations (e.g., Na<sup>+</sup>, K<sup>+</sup>, Ca<sup>2+</sup>) to membrane fusion (e.g., H<sup>+</sup>, Ca<sup>2+</sup>, Mg<sup>2+</sup>, Zn<sup>2+</sup>, Cu<sup>2+</sup>). Experimental molecular-level interfacial studies of ions in contact with LMs,<sup>34,70,71</sup> SLBs<sup>72</sup> and modeling<sup>62,73</sup> have shown that ion-membrane interactions are currently understood to be a consequence of an interplay of ion pairing, partitioning of ions to the water/hydrophobic interface, steric effects and counterion interactions. As an example, in Figure 2A, a combination of sum frequency generation (SFG) and molecular dynamics (MD) simulation study<sup>62</sup> has examined the molecular conformation of lipid head groups in a uniform bilayer (MD) as a function of Ca<sup>2+</sup> concentration. It was found in the MD studies that even though the PS headgroup is charged (and should therefore interact strongly with Ca<sup>2+</sup> ions) its tilt angle depends only very weakly on the Ca<sup>2+</sup> concentration. The PC headgroup, on the other hand, displays a strong dependence on Ca<sup>2+</sup> concentration.<sup>62</sup> While the SFG data on LMs at the air/water interface changed as a function of Ca<sup>2+</sup> concentration, a comparison about tilt angles could not be made, due to the difference in system. The probing of FLMs with SFG, which would allow direct comparison to the MD results, has not been achieved since the bulk aqueous solution adjacent to each leaflet forms a barrier to the optical infrared (IR) probe. In addition, how local variations in the membrane topography or other constituents or presence of mixed membrane structures affect the observed behavior is yet to be investigated.

Although many computational studies exist that address the question of how membrane proteins such as pores and channels operate<sup>74,75</sup> (see, e.g., cited work in ref 76), experimental molecular-level/hydration information on functioning proteins has not been achieved so far. However, as a start, the structure/interaction of proteins and channels with LMs and SLBs is attracting much interest in the field,<sup>72,77</sup> yet to achieve this goal numerous experimental conditions must be well-controlled, such as passivation of the solid support surface to minimize possible membrane protein denaturation. One recent example concerns recent reflection-SFG studies on artificial pores that were inserted in 4:1 PC/PS SLB deposited on a silica/water interface,<sup>68</sup> see Figure 2B. The chiral assembly of the pore forming molecules is superimposed to the water molecules transporting through the pores, by unambiguously detecting chiral SFG response in the vibrational O–H stretch region. How much of this response is due to the silica support is not clear, however. Nevertheless, that the channels imprint their chirality on water is a surprising

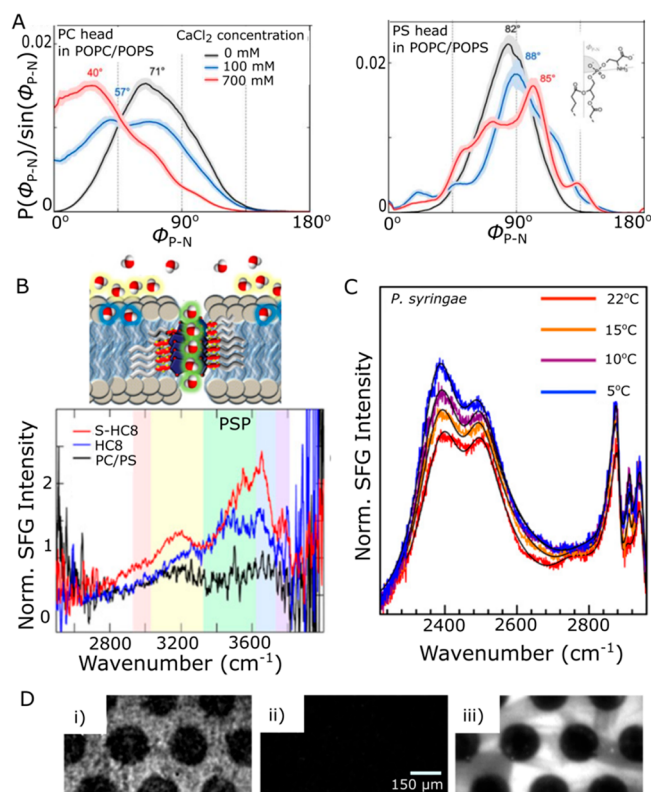


**Figure 2.** State of the art molecular-level interfacial membrane information. (A) The normalized (P–N) headgroup tilt angles with respect to the surface normal for a mixed POPC/POPS bilayer membrane in aqueous solution as a function of CaCl<sub>2</sub> concentration. The PC headgroup (left panel) and the PS headgroup (right panel) tilt angles are shown. A small Ca<sup>2+</sup> dependence can be seen for the PS headgroup, while a much larger Ca<sup>2+</sup> dependence is observed for the PC headgroup. Adapted from ref 62. (B) Probing chiral water in artificial nanopores: chiral SFG spectra of the O–H stretch region for 4:1 PC/PS SLB (black trace), and the same SLB including HC8 (blue trace) and S-HC8 (red trace) I-quartet pores. The cartoon illustrates the experiment and the green highlighted water molecules indicate the source of the chiral water signal. (C) Temperature dependent SFG spectra of *P. syringae* bacteria lysate containing ice-active inaZ proteins. Temperature dependent water signal increase can be seen only with the presence of ice-nucleating proteins. Adapted from ref 80. (D) Confocal resonant chiral-SH imaging of arrays of structured POPC supported lipid bilayer. (i) SBN, (ii) a racemic mixture of RBN and SBN and (iii) a fluorescent microscopy image of a different bilayer labeled with Rh-DOPE. Panel A is adapted from ref 62 published by Springer Nature with a Creative Commons License. Panels B and C are adapted from reference 68, 80 with permission from exclusive licensee American Association for the Advancement of Science, distributed under a Creative Commons Attribution Non-Commercial License 4.0 (CC BY-NC). Panel D is reproduced from ref 81 with permission of the American Chemical Society. Figure abbreviations: HC8 = octylureido-ethylimidazole, S-HC8 = S-octylureido-ethylimidazole, PC = phosphocholine, PS = phosphoserine, POPC = 1-palmitoyl-2-oleoyl-*sn*-glycero-3-phosphocholine, POPS = 1-palmitoyl-2-oleoyl-*sn*-glycero-3-phosphoserine, Rh-DOPE = Rhodamine-1,2-dioleoyl-*sn*-glycero-3-phosphoethanolamine, DPPC = 1,2-dipalmitoyl-*sn*-glycero-3-phosphocholine. RBN and SBN = R- and S-(+)-1,1'-bi-2-naphthol.

effect, and one that emphasizes the intimate link between water and biomolecules. Other studies have shown that water molecules follow the chirality of an array of DNA molecules that was crafted to a surface.<sup>78,79</sup>

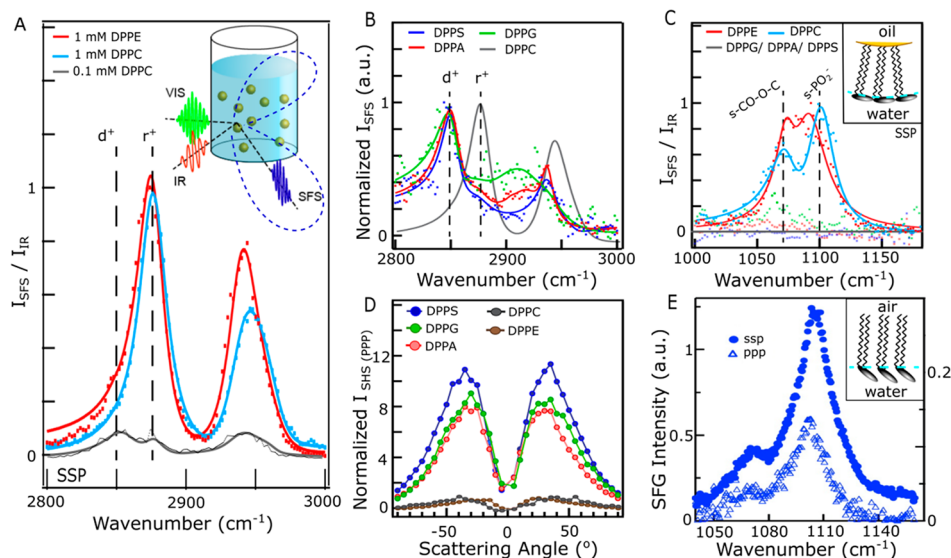


**Figure 3.** Molecular interfacial structure of nanoscale lipid droplets. (A) SFS spectra of the C–H stretching region of 1 mM DPPC (blue), 0.1 mM DPPC (gray) and 1 mM DPPE (red) monolayers on 100 nm-radius  $d_{34}$ -hexadecane nanodroplets (2 vol %) in  $D_2O$ . The inset shows the SFS process. (B) Normalized SFS spectra of 1 mM DPPS (blue), 1 mM DPPG (green), 1 mM DPPA (red) and 1 mM DPPG (gray) monolayers on oil ( $d_{34}$ -hexadecane) nanodroplets (2 vol %) in  $D_2O$  for the C–H stretching modes. (C) SFS spectra in the P–O stretch region of the vibrational spectra for DPPE (red curve), DPPC (blue curve), as well as DPPG (green), DPPA (orange) and DPPS (purple) data points, all associated with the gray fit. The inset shows the head groups are aligned away from the surface normal. (D) Normalized AR-SHS patterns of oil nanodroplets with charged DPPS (blue), DPPG (green) and DPPA (red), as well as zwitterionic DPPC (gray) and DPPE (brown) monolayers. Differences in the number density and size of nanodroplets between different samples are corrected. The inset shows the more packed lipid headgroup area for lipid monolayers at the air/water interface. The figure is adapted from refs 45, 53, 57, 58 with permission from the American Chemical Society. Figure abbreviations: DPPC = 1,2-dipalmitoyl-*sn*-glycero-3-phosphocholine, DPPE = 1,2-dipalmitoyl-*sn*-glycero-3-phosphoethanolamine, DPPS = 1,2-dipalmitoyl-*sn*-glycero-3-phosphoserine, DPPG = 1,2-dipalmitoyl-*sn*-glycero-3-phosphoglycerol, DPPA = 1,2-dipalmitoyl-*sn*-glycero-3-phosphate.

Another example of understanding the molecular-level picture of membrane processes is the temperature dependent study of ice-nucleating proteins, depicted in Figure 2C. The lysate of the *Pseudomonas syringae* bacteria containing ice-active inaZ protein demonstrates a progressively increasing water signal with decreasing temperatures. Moreover, the temperature dependent change of the SFG signal disappears for the control samples such as DPPG monolayers, and lysozyme proteins, indicating that the ice nucleating protein indeed changes the water structure.<sup>80</sup> One may ask if it is this unique, and if the reverse is also the case (i.e., water dictating protein structure). Whether water dictates protein structure, however, is more difficult to study and has, therefore not been reported.

Since ion, molecular and single protein specific modeling requires atomistic models, and spectroscopic techniques typically record spatially and temporally averaged information, our understanding is either localized to atomistic detail from simulations or averaged over time and space into crude mean field models that have no explicit atomic details embedded in them. Adding the spatiotemporal dimension requires non-invasive label-free interface specific microscopy tools with molecular specificity. To this end static resonant SH imaging<sup>81–84</sup> and SF imaging<sup>85–88</sup> have been developed. Studies on monolayers and on lipid bilayers are few.<sup>19,43</sup> Figure 2D shows the confocal chiral-SHG images of chiral molecules (i), as well as a racemic mixture of the same molecules (ii) in a POPC supported lipid bilayer. The first SH image shows a contrast arising from the chiral nonlinear optical response, while the second image does not. Image (iii) is a fluorescent control image to colocalize the chiral molecules.

This shows that the chiral molecules in the supported bilayer membrane interface can be imaged with resonant SH imaging.<sup>19,81</sup> These results are promising, but due to the weak nonlinear optical response in these experiments, recording times are more than 20 min per image. Since structural changes relevant for chemistry and biology occur on much shorter millisecond time scales, no dynamic information can be obtained.

Having given an overview and flavor of the state of the art pertaining to the molecular-level interfacial investigation of LMs and SLBs, and having highlighted some of the limitations of this approach to understand the aqueous chemistry of membranes, we now turn to recent advances concerning the molecular-level interfacial understanding of more realistic free-floating nano-, micro- and macroscopic membranes in solutions which leads us even to the molecular-level investigation of active neuronal cell membranes. We pay particular attention to effects of size, curvature and confinement, hydration, electrostatics and the emerging role of spatiotemporal heterogeneities.

**Nano- and Microscale Membrane Model Systems.** To increase the complexity toward more realistic membrane systems in the quest toward a full scale molecular-level membrane understanding, one approach is to probe molecular interfacial structure on small objects in turbid solutions, such as lipid droplets and liposomes. In our laboratory, we have developed vibrational sum frequency scattering (SFS)<sup>89</sup> and nonresonant angle resolved (AR) second harmonic scattering (SHS).<sup>90</sup> Before advancing to the 3D membrane systems, both techniques are first briefly introduced.

**Nonlinear Optical Methods for Probing 3D Interfaces in Solution.**

A full description of the second-order nonlinear light scattering techniques used here is beyond the scope of this Perspective. For a detailed description of these methods, see ref 50, for an educational review, ref 91, for sum frequency scattering in particular and refs 13, 60 for second harmonic scattering. Vibrational SFS, invented by Roke,<sup>89</sup> (Figure 3A) is a combination of vibrational sum frequency spectroscopy and light scattering. SFS is inherently surface sensitive for isotropic bulk media, which makes it a valuable tool to obtain chemical structural information on interfaces in suspension. Figure 3A shows an illustration of a vibrational SFS experiment: visible (VIS) and infrared (IR) pulses are spatially and temporally overlapped in a suspension of nanodroplets/liposomes. The sum frequency (SF) photons originate from a simultaneous Raman and infrared transition. Since simultaneous Raman and infrared activity is only possible in the absence of local molecular inversion symmetry, SFS takes place exclusively at the droplet, liposome or membrane surface (i.e., in absence of charge within a spherical shell with a thickness <1 nm), where such inversion symmetry is broken. The SF light is scattered in a 3D angular distribution, determined by the size of the objects (typically the radius), the surface structure (as captured by the second-order susceptibility,  $\chi_s^{(2)}$ ) and the interfacial electrostatic landscape (as captured by the surface potential,  $\Phi_0$ ).<sup>13,50,60,92</sup> The sensitivity to interfacial processes is much enhanced compared to traditional reflection SFG experiments from extended planar interfaces as nanodroplet/liposome solutions have a surface to volume ratio that is typically 3 orders of magnitude larger than that of a planar interface. Further, since the liquid interfaces are prepared in situ in the probing medium with a very high surface to sample volume ratio, contaminations or film defects are no issue.<sup>93</sup> SFS has been applied to study the structure of a wide range of interfaces, both in aqueous and nonaqueous liquids, ranging from oil in water<sup>91,94–98</sup> and water in oil emulsions,<sup>99</sup> to colloidal particles,<sup>89</sup> cationic surfactant vesicles,<sup>101</sup> to embedded solid clusters in amorphous materials,<sup>100,102</sup> biopolymers in solution<sup>103</sup> and cellulose structures.<sup>104</sup>

SHS (Figure 3A) with both beams being of the same near-infrared frequency) has been used to measure surface properties of particles in liquids since 1996.<sup>105</sup> SHS is the frequency degenerate form of SFS and has mostly been performed on-resonance using chromophores (see refs 50, 106 for reviews). The chromophores that have shown most promising results are malachite green<sup>105,107,108</sup> and crystal violet.<sup>109,110</sup> Using these markers, liposomes membranes and ion penetration through them<sup>111</sup> were investigated as well as the transport of ions through bacterial membranes.<sup>112</sup>

Recently, our laboratory has made significant improvements to the experimental implementation of SHS, improving the throughput of the SHS instrument by several orders of magnitude.<sup>90</sup> This was achieved by optimizing the trade-off between energy transfer and SH generation efficiency in aqueous solutions, and enables the nonresonant probing of water molecules at nanoscopic aqueous interfaces on sub-second time scales. Despite the lack of chemical specificity, the probing of water is made possible by the number density of interfacial water molecules compared to other dipolar species that can generate a nonlinear source polarization. As the SH intensity scales quadratically with the surface density of dipolar species and since the nonresonant response is determined by hyperpolarizability values that are of the same order of

magnitude, in many cases (and certainly in the case of lipid droplets and liposomes) the SHS response reflects the interfacial water structure.

**Lipid Droplets.** With SFS and SHS it is possible to determine interfacial structural properties of lipid droplets. Figure 3B shows SFS spectra of hexadecane oil droplets with an interfacial layer of lipids (DPPC and DPPE) in water with varying lipid densities.<sup>53,57</sup> This system can be easily prepared by mixing the desired amount of lipid oil and water, and subsequently homogenizing and sonicating it. By measuring SFS spectra of both the acyl chains and the headgroup vibrational modes, we found that lipid monolayers with a tunable density varying from molecular areas and tilt angles from 0.48 nm<sup>2</sup> and 30° to 0.8 nm<sup>2</sup> and 70° could be formed.<sup>53</sup> The molecular structures of various other 3D phospholipid monolayers consisting of different zwitterionic PC head groups with different acyl chains were also investigated.<sup>58</sup> Shortening the lipid tail length introduces more disorder (gauche defects) to the 3D lipid monolayers, and the monolayer packing becomes more disordered. For unsaturated 1,2-dioleoyl-*sn*-glycero-3-phosphocholine (DOPC) and single acyl chained 1-palmitoyl-2-hydroxy-*sn*-glycero-3-phosphocholine (lyso-PC) lipids, the monolayer packing becomes more disordered. The single tailed lyso-PC lipid forms “patchy” monolayers.<sup>53,57,58</sup> In contrast to the 3D monolayers of zwitterionic lipids such as DPPC and DPPE (Figure 3B), monolayers of charged lipids (such as with phosphatidylserine (PS), phosphatidic acid (PA) and phosphatidylglycerol (PG) head groups) form remarkably different monolayer structures.<sup>57</sup> This is illustrated in Figure 3B,C where the C–H mode acyl tail and headgroup P–O region are shown for both the zwitterionic and charged lipids: The zwitterionic lipids display strong SF responses with the methyl stretch mode as the dominant vibrational mode (Figure 3B, gray trace), while the charged lipids display a very low intensity with a vanishing methyl mode response (Figure 3B, blue, green and red data). For the headgroup region, the response for the P–O stretch mode is either strong (Figure 3C, blue and red data) or absent (Figure 3C, green, orange and purple data). This means that zwitterionic lipids can pack into dense geometric films while the negatively charged DPPS, DPPA and DPPG lipids form 3D monolayers with a very low number density, completely disordered acyl tails and head groups that stick into the solution. The SHS response (Figure 3D) for both zwitterionic and charged lipids follows the opposite trend: a high intensity is observed for charged lipids, while a low intensity is observed for the zwitterionic lipids. This is interpreted to arise from a difference in oriented water. PC/PE lipids orient water molecules in plane along the P–N axis, which does not give rise to a detectable SH response, while charged lipids can orient water molecules along the normal direction via charge–dipole interactions, leading to a strong SH response.<sup>53,57,113</sup> Compared to planar extended interfaces, these structures are different. Figure 3E shows headgroup spectra of DPPC molecules at the air water interface. Here, the tilt angles are larger with respect to the surface normal giving rise to a more densely packed film.<sup>45</sup>

**Liposomes.** Liposome interfaces have also been investigated with SFS and SHS. The structure of these ideal lipid bilayers is thought to be composed of lipids with a constant lipid headgroup area in each leaflet, combined with identical hydration.<sup>114</sup> To verify this molecular-level picture, single lipid component liposomes in aqueous solutions were probed with SFS and AR-SHS.<sup>13,14,59</sup> For membranes that have two

oppositely oriented leaflets, the SFS amplitude reports on the transmembrane asymmetry in the number of lipids per leaflet. For 100 nm liposomes, the outer leaflet has a larger area than the inner one. For a geometric packing to occur, there should be an excess of 8% of lipids on the outside leaflet, giving rise to an SFS response in both the headgroup (P–O) and acyl chain (C–H) responses. However, we found that the SFS spectra of single component unilamellar vesicles (~100 nm in diameter, composed of DPPC, DOPC, DPPS) show no detectable intensity for both the C–H and the P–O modes. An example spectrum is shown in Figure 4A. With a detection limit of the SFS technique corresponding to 2% lipid asymmetry,<sup>59,93</sup> there is virtually no trans-membrane asymmetry for either the hydrophobic core or the headgroup region.

Since SFS detects the same number of lipids in the inner and outer leaflets, while there must be an area difference between the inner and outer leaflets, another candidate for filling up this volume is water. This was measured with AR-SHS. Figure 4B shows normalized<sup>115</sup> AR-SHS patterns<sup>59</sup> of single component unilamellar vesicles (100 nm, composed of DOPC, DPPC and DPPS). The SHS intensity signal is nonzero for all liposomes, demonstrating that the hydration environment of the inner leaflet is different from the outer leaflet. Moreover, charged DPPS liposomes generate ~21 times more SHS intensity per liposome compared to the zwitterionic liposomes. This difference can be explained by the interaction of the electrostatic field of the headgroup charges on the outer leaflets with the adjacent water molecules. This charge–dipole interaction induces changes in the orientational distribution of the interfacial water molecules and hence increases the SHS intensity. In the inner leaflets this effect is less since there can be no electrostatic gradient in the center of the liposomes (as described more in detail further below). Zwitterionic leaflets do not possess free charges, and thus the SHS response likely arises from a difference in hydrogen bond interactions. This hydration asymmetry between the leaflets of liposomes sheds new light on X-ray and neutron scattering measurements that reveal an asymmetrically trans-membrane distribution of electron density on anionic vesicles.<sup>116</sup>

Real lipid membranes are much more complex in terms of membrane composition than just single component liposomes. To test the influence of multiple lipid species, the interfacial structure of liposomes composed of binary lipid mixtures were also explored. Figure 4A shows SFS spectra of liposomes in the P–O stretch region composed of a 1:1 mixture of DOPC-DPPS and DOPS-DPPC. It can be seen that the DOPC-DPPS liposomes generate a nonzero SFS spectrum in the headgroup region. Interestingly, only a single peak at ~1080 cm<sup>-1</sup> is observed for the mixed lipid liposomes. In comparison with the SFS spectra of any measured zwitterionic PC monolayer on the surface of oil nanodroplets, this peak position is 20 cm<sup>-1</sup> red-shifted.<sup>57</sup> Such a red peak shift reports on changes in intermolecular and H-bonding interactions as well as the local aqueous environment.<sup>45,57,118</sup> Thus, it is most likely assigned to a population of s-PO<sub>2</sub><sup>-</sup> stretch modes that are H-bonded with the NH<sub>3</sub><sup>+</sup> group of the neighboring PS lipids. Other binary lipid liposomes such as DOPS-DPPC, on the other hand, that do not have this type of interaction do not display lipid headgroup asymmetry.<sup>39</sup>

These first results on probing the molecular structure of lipid droplets and liposome interfaces in aqueous solution thus show already a surprising number of differences with LMs and SLBs, regarding to the structure of the interface. These structural

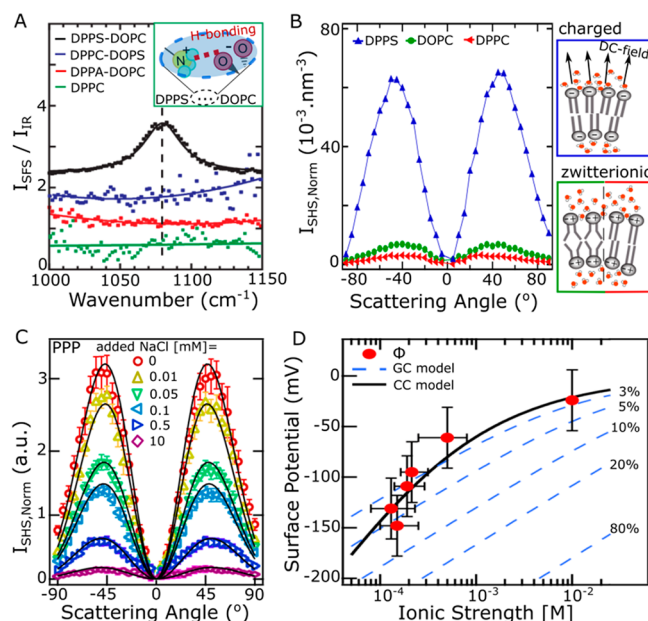


**Figure 4.** Molecular interfacial structure of liposomes in solution. (A) SFS spectra of the P–O stretch region of liposomes (100 nm diameter) in D<sub>2</sub>O composed of DPPC lipid (green), 1:1 mixtures of DOPC-DPPS (black), DOPS-DPPC (blue) and DOPC-DPPA (red). The inset illustrates H-bonding interaction between the DPPS and DOPC lipids, which gives rise to membrane asymmetry. (B) Hydration asymmetry between membrane leaflets as probed by AR-SHS of DPPS (blue), DOPC (green) and DPPC (red) liposomes in pure H<sub>2</sub>O. The scattering pattern originates from the overall transmembrane asymmetry in the orientational distribution of water molecules around the lipids (as illustrated in the cartoons on the right side of the figure). (C) The AR-SHS patterns from DOPS liposomes as a function of ionic strength measured in PPP polarization combination. Ionic strength of the samples are indicated in the legend. The error bars represent the standard deviation of 20 measurements. (D) The extracted surface potential vs ionic strength. Error bars consider the standard deviations for  $\chi_{s,2}^{(2)}$  the number density, and the radius. The dashed blue lines represent surface potential values calculated with the Gouy–Chapman (GC) model for spherical particles<sup>119</sup> using different surface charge densities  $\sigma_0$  (indicated as degree of ionization of the DOPS head groups in the outer leaflet). The solid black line represents a fit using the spherical constant capacitor (CC) model. Neither model describes the measurement. The figure is adapted from refs 13 and 59 with permissions from the American Physical Society and American Chemical Society, respectively. Figure abbreviations: DPPC = 1,2-dipalmitoyl-*sn*-glycero-3-phosphocholine, DPPE = 1,2-dipalmitoyl-*sn*-glycero-3-phosphoethanolamine, DPPS = 1,2-dipalmitoyl-*sn*-glycero-3-phosphoserine, DPPG = 1,2-dipalmitoyl-*sn*-glycero-3-phosphoglycerol, DPPA = 1,2-dipalmitoyl-*sn*-glycero-3-phosphate, DOPC = 1,2-dioleoyl-*sn*-glycero-3-phosphocholine, DOPS = 1,2-dioleoyl-*sn*-glycero-3-phosphoserine.

differences suggest that there may also be differences in terms of interactions. As electrostatic and hydrogen bonding interactions are chemically the most determining interactions, we next turn our attention to quantifying interfacial electrostatics using second harmonic scattering.

**Electrostatic Membrane Potential.** SH scattering patterns emerge as a consequence of the ratio of the size of the object compared to the wavelength of the probing beams. When the object and wavelength are of the same order of magnitude, the optical beams will induce a second-order polarization that has a different phase and magnitude on each

point of the object. Every point of the object will be a source for the emission of second-order light, and the resulting interference pattern is the finally measured scattering pattern.<sup>50,115,120,121</sup> This SH intensity pattern, for a single scattering object, depends on the size (size<sup>6</sup> for spherical shells <200 nm<sup>115</sup>), the molecular interfacial structure (via  $\chi_{s,2}^{(2)}$ ), and the interfacial electrostatic potential,  $\Phi_0$ .<sup>13,60</sup> Although it was already recognized in the 1960s that the SH intensity relates to the interfacial electrostatic potential,<sup>122</sup> and it was shown by the Eisenthal group that the forward scattered SHS intensity from liposomes connects empirically to the surface potential,<sup>117,123</sup> it has only recently become possible to determine unique surface potential values from SHS experiments: The full AR polarimetric scattering process can be described by treating the electrostatic interfacial field as one of the participating optical fields (with a frequency  $\omega = 0$ ) in the nonlinear optical expressions.<sup>60</sup> Using this three wave process ( $\omega + \omega + 0 = 2\omega$ ), unique intensity expressions can be described for different polarization combinations of the incoming and outgoing beams. For isotropic spheres, and nonresonant SHS there are two independent intensity expressions with two independent parameters ( $\chi_{s,2}^{(2)}$  and  $\Phi_0$ ), allowing the measurement of a unique value of the surface potential.<sup>13</sup> This is a unique method as it is the first method that does not require a model (such as the Gouy–Chapman or Gouy–Chapman–Stern models) to describe the interfacial electrostatics of a dilute solution of nano- and microscale particles. In contrast to other methods (e.g., electrokinetic mobility measurements<sup>124</sup>), no mean-field assumptions about the interfacial structure are needed and the surface potential is measured at the plane of the interface (as opposed to a plane some unknown distance away from the interface, such as the slipping plane). A recently proposed synchrotron based X-ray photoelectron spectroscopy (XPS) procedure<sup>125</sup> uses electronic energy differences related to the Fermi level in solution and is applicable to concentrated (5 wt %) nanooxide particle (<9 nm) solution. Compared to this approach, AR-SHS allows for dilute (<5 vol %) solutions of a wide range of sizes ( $\sim$ >20 nm), in a high-throughput table-top setup,<sup>90</sup> and is applicable to soft matter interfaces such as lipid droplets and vesicles.

Recent polarimetric angle resolved second harmonic scattering measurements were performed on different liposome systems.<sup>13</sup> Figure 4C,D shows examples of the obtained AR-SHS scattering patterns of DPPS liposomes as a function of ionic strength and the retrieved membrane surface potential values, respectively. Figure 4D also includes the predictions of membrane potentials calculated using different mean field models. These potential values differ from potentials obtained from planar systems. As can be seen in the figure, the obtained liposome membrane potential values roughly follow the modeled trend but do not agree with the mean field theory. The reason for that is that charge condensation,<sup>14</sup> degree of interfacial ionization,<sup>13</sup> the presence of a patchy Stern layer,<sup>97,98</sup> and the amount of order in the interfacial hydrogen bond network<sup>126</sup> all appear to depend on both the local molecular chemical environment as well as the curvature/size of the system. This information is of course not available in a mean field model.

**Length Scale and Curvature.** The above findings about structure and hydration in the section [Nano- and Microscale Membrane Model Systems](#) and electrostatic interactions in the section [Electrostatic Membrane Potential](#) suggest that on different length scales the balance of interactions (electrostatic,

hydrogen bonding, dipole–dipole interactions and entropic effects) is different, and critically depends on the chemical composition of the lipids and size of the system, leading to different physicochemical properties. Similar results were found in studies on nanoemulsions of oil droplets in water that display low saturation charge densities that are more than 1 order of magnitude less than equivalent planar interfaces.<sup>94,113,127</sup> This peculiar observation is explained by a different balance of interactions.<sup>113</sup> Charged surfactants adsorb to the oil/water interface, and interact with the other surfactant molecules in solution and with the other surfactants that are also adsorbed to the interface. Since the oil phase (having an ionic strength of <1 nM) does not screen the charges of the surface-absorbed surfactant molecules, there is a repulsive barrier toward forming a dense geometric film of surfactant molecules. The balance of interaction is expected to change to bulk-like interactions as the droplets reach a diameter of several microns. The reverse system, water droplets dispersed in a hydrophobic liquid, was also investigated with SFS.<sup>99</sup> These water droplets were stabilized with a neutral noncharged surfactant, and the interfacial hydrogen bond network displayed an unusually large order, corresponding to a temperature decrease of  $\sim$ 50 K. These examples clearly demonstrate that the balance of interactions is substantially different at the nanoscopic length scale compare to macroscopic length scales.

In the case of liposomes, the fact that there is structural water asymmetry (but no lipid asymmetry) shows that the bilayer in a 100 nm diameter liposome is differently structured than a planar extended bilayer (for which there is no average water asymmetry<sup>15,43</sup>). This has been observed for both charged and zwitterionic liposomes (Figure 4A and refs 14, 59), and it is not clear over which length scale this behavior persists. Likewise, there is no formal knowledge on the electrostatic environment inside a small liposome. On an extended planar bilayer interface, mobile charges at the interface and in solution give rise to an electric double layer that screens charges and determines local structure and reactivity. Curving such a bilayer to the size of an SUV or LUV bends this double layer and produces an electrostatic field gradient directed toward the center of the liposome. At the same time, however, electrostatics predicts by virtue of Gauss' law that there can be no electric field at the center of the liposome.<sup>128</sup> Also, as charges and water molecules are confined to a smaller space the balance of driving enthalpic and entropic interactions changes compared to a planar extended bilayer in aqueous solution. Because the length scale of SUVs and LUVs is too large for atomistic modeling and too small or heterogeneous to be captured by mean field models, there is no analytical model to describe this situation.<sup>129</sup> To obtain a better insight on the effects related to length scale, it is necessary to also probe membrane structure, hydration and the various types of interactions on macroscopic free-floating membranes ideally with the ability to connect to submicrometer length scales and subsecond resolution.

**Spatiotemporal Imaging of Membrane Water: Heterogeneity.** In order to connect submicrometer length scales with subsecond time scales, one needs imaging approaches that are sensitive to the weak optical or nonlinear optical responses of water, and at the same time sensitive enough to do this on a subsecond time scale. Vibrationally resonant coherent anti-Stokes Raman scattering has been used to image with great success mostly lipid,<sup>119,124,130</sup> but also water permeability.<sup>125</sup>

Direct visualization of the arterial wall water permeability barrier using coherent anti-Stokes Raman scattering microscopy.<sup>125,131</sup> Real-time visualization of intracellular hydrodynamics in single living cells has also been observed.<sup>131,132</sup> Ordering of water molecules between phospholipid bilayers has been visualized by coherent anti-Stokes Raman scattering microscopy.<sup>132</sup> However, the third-order nature of the nonlinear optical process prevents interface specificity, which is inherently available with second-order techniques. The recent invention of high-throughput wide field SH imaging<sup>84,133</sup> in our laboratory has made it possible to SH image interfacial hydration and to derive spatial maps of surface potentials and chemical reaction constants of glass/water interfaces,<sup>133</sup> and more recently from lipid bilayer membrane/water interfaces.<sup>15</sup>

Figure 5A shows a simple schematic of the imaging approach where two near-infrared fundamental pulsed femtosecond

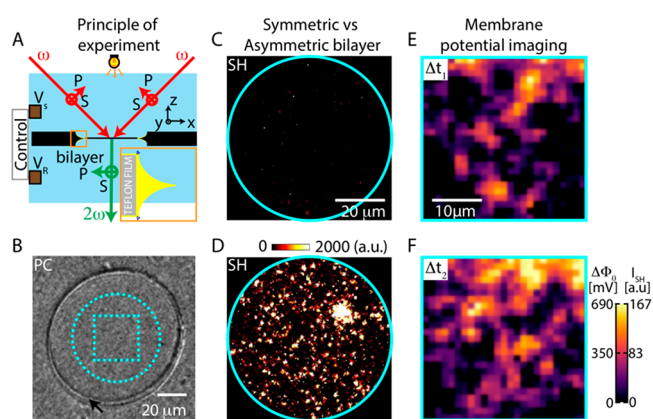


**Figure 5.** Spatiotemporal imaging of membrane water. (A) Principle of the experiment on FLMs, and (B) phase contrast image of a FLM. (C, D) SH emission is only visible from an interface that has broken spatial symmetry along the surface normal: SH image of a symmetric (DOPC) FLM (C) and SH image of an asymmetric membrane having a charged (top) leaflet composed of DPPS:DOPC:Chol, and a neutral (bottom) leaflet composed of DPPC:DOPC:Chol. (D). The charged lipids are primarily distributed into domains. (E, F) Dynamic membrane potential imaging: snapshots at different time intervals of the same segment (indicated in B) of an asymmetric FLM composed of DPhPC:DPhPS mixture (top) and DPhPC (bottom). Spatial and temporal fluctuations of several hundreds of millivolts are seen (the average membrane potential is  $-50$  mV). The figure is adapted from ref 15 that is published at the Proceedings of the National Academy of Sciences of the USA under a CC BY-NC-ND license. Figure abbreviations: DOPC = 1,2-dioleoyl-*sn*-glycero-3-phosphocholine, DPPS = 1,2-dipalmitoyl-*sn*-glycero-3-phosphoserine, Chol = cholesterol; DPPC = 1,2-dipalmitoyl-*sn*-glycero-3-phosphocholine, DPhPC-1,2-diphytanoyl-*sn*-glycero-3-phosphocholine, DPhPS-1,2-diphytanoyl-*sn*-glycero-3-phosphoserine.

beams are overlapped on an FLM interface. SH photons are emitted from the  $\sim 100$   $\mu\text{m}$  wide illuminated area in the phase matched direction. This wide field geometry allows for probing all 8 possible polarization combinations, with a spatial resolution of 380 nm and a temporal acquisition time of  $\sim 250$  ms, short enough to probe interfacial dynamics relevant for biological processes. The FLM consists here of a macroscopic  $\sim 6$  nm thick lipid bilayer that is contained within a  $\sim 100$   $\mu\text{m}$  wide circular aperture of a thin Teflon film. Such lipid bilayers have been reported since 1972<sup>134</sup> and have been characterized mainly via their electrical resistance and

capacitance.<sup>135–137</sup> They are widely used membrane model systems as they can be prepared with various lipids and the lipids can be distributed asymmetrically via the Montal-Mueller preparation procedure.<sup>15,134</sup> Compared to LMs and SLBs, such FLMs have the advantage that they are full bilayers that are completely surrounded by an aqueous phase on both sides, excluding any sort of substrate artifacts induced by the substrate, or changes in elastic or mechanical properties. They are thus closer to a real biological membrane, and can be dressed up to mimic one by adding key constituents.

Figure 5B shows a white light phase contrast (PC) image from an FLM, with its characteristic Newton fringes. SH imaging the FLM from the top, optical contrast emerges only when the lipid bilayers are structurally asymmetric along the surface normal. Figure 5 shows an example of a SH image of a symmetric (Figure 5C) and an asymmetric bilayer (Figure 5D). The origin of the SH contrast observed in the asymmetric image was traced back by a series of experiments<sup>15</sup> involving the addition of ions to solution and the changing of pH to the following source: interfacial water molecules that have changed their orientation as a consequence of the interaction with the charged lipid head groups. Figure 5E and 5F show SH images taken at two different time intervals 2 s apart. A series of such images can be cropped into spatiotemporal interfacial hydration videos. Combining SHM with nonlinear optical theory, membrane potential maps were generated. The average potential found from these maps corresponded well with the value found by capacitance minimization. The SH images in Figure 5E,F show the derived membrane potential on the scale bars. It can be seen that spatial and temporal fluctuations in the electrostatic energy landscape are observed to be as large as 600 mV, equivalent to  $\sim 20$  kT. The length scale of the fluctuations comprises a few micrometers. These results imply that mean field models that are still sufficient to understand simplistic monolayer and bilayer systems fail to capture this type of findings, potentially because of the use of spatial and temporal averaging that is long enough to eliminate fluctuations. However, since the fluctuations connect to potential energy landscape maxima and minima, they are essential for understanding chemistry.

This surprising finding suggests that the electrostatic environment within the interfacial water layer is dynamic. It may influence a wide variety of phenomena that depend upon the electrostatic energy landscape, including the interaction of lipids and membranes with ions, membrane-protein interactions, membrane structural fluctuations (such as the formation of transient structures), the transport through the membrane, membrane mechanical properties, membrane fusion and the working of pores and channels. For example, the potential difference needed to create a transient pore in a lipid membrane is between 150 and 600 mV.<sup>138</sup> Given that the values measured here are in this range, it could well be that these membrane potential fluctuations are responsible for opening up tiny transient pores. These tiny pores would be responsible for small amounts of water and ion transport. Indeed, several studies have suggested that this is the case,<sup>139</sup> based on electrical current measurements,<sup>140,141</sup> but no explanation has been found. Our data suggest that the intrinsic fluctuations in the hydration structure of the membrane might be the cause. Connections to other spatiotemporal degrees of freedom such as membrane stiffness may also be present, but all of this has yet to be investigated.

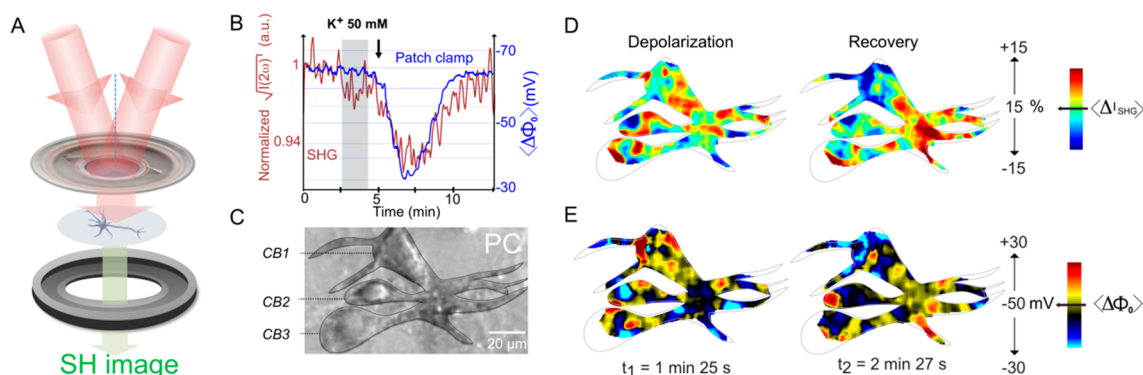


**Figure 6.** Water as a contrast agent for neurological activity. (A) Imaging configuration of neurons. The neurons are provided with a constant flow of solution via a peristaltic perfusion system and SH imaging is done in a wide-field double beam transmission geometry. The incoming beams (red arrows), and the emitted second harmonic (SH) photons (green arrow), the imaging plane contains the neurons (blue plane). (B) The square root of the second harmonic (red, left y axis) response that is proportional to the membrane potential and electrophysiological response (blue, right y axis) during  $K^+$  ion-induced depolarization follow identical patterns as a function of time. (C) A phase contrast image of 3 neuronal cell bodies. (CB1, 2 and 3 indicate 3 different cell bodies). (D) Images of the percentile change in the SH response at two different times in the membrane depolarization cycle. (E) Images display the corresponding membrane potential maps. The figure is adapted from ref 146, which is published at Springer Nature under a Creative Commons license.

**Membrane Potential Imaging in Living Neurons.** With the ability to generate label-free membrane potential maps using the interfacial water molecules as an in situ “contrast agent”, it becomes possible to gain new insights in biological systems. Especially for cells and tissues that depend on membrane potential fluctuations, such as the nervous system or cardiac cells. Previous studies<sup>142,143</sup> using a variety of fluorescent membrane potential sensitive markers have shown the great potential of SHM for neuroscience, but the toxicity of the probes or the need to resort to genetic modification<sup>144,145</sup> remains a disadvantage. To explore this exciting avenue of using water as a contrast agent (nontoxic and present everywhere), we have recently started probing neurological activity using our wide field high throughput SHM. Figure 6A shows a sketch of the optical layout. In these experiments, primary cortical mouse brain neurons were placed on a glass coverslip under flow of an appropriate medium. To confirm the expected linear relationship between electrostatic potential and the square root of the SH response also in living cells, side by side patch clamp and SH imaging measurements were performed while the resting potential was modified by a  $K^+$  induced depolarization process. Indeed, Figure 6B shows a linear correlation between the electrostatic potential measured by a patch clamp (y axis right, blue trace) and the optically determined square root of the SH intensity (y axis left, red trace, whole cell averaged) that is proportional to the membrane potential. In the next step, we converted the intensity to membrane potential values,<sup>146</sup> leading to snapshots of the membrane potential with 600 ms temporal resolution. Figure 6C shows a phase contrast image of 3 cell bodies, and Figure 6D,E displays the change in the SH response and the corresponding membrane potential changes for both depolarization (adding additional  $K^+$  ions to the extracellular liquid, left), and repolarization (removing the excess of  $K^+$  ion, right).  $K^+$  ion flux maps were also created based on the known relationship between charge flow ( $dQ/dt$ ) and membrane potential ( $Q = C\Delta\Phi_0$ ). While the average temporal response agrees with the theoretically expected membrane potential changes and the electrophysiological recordings obtained with the same protocol, the images show clear spatiotemporal fluctuations within the neurons. It can be seen that different

parts of the cells (soma or neurites) are active at different parts of the depolarization cycle. Thus, there is not only a nonuniform distribution and density of permeant ion channels but also different temporal activity. There could be a connection to the observed fluctuations in membrane potentials of FLMs (see [Spatiotemporal Imaging of Membrane Water: Heterogeneity](#) section) but this needs to be further explored by performing more extensive bottom-up and top-down studies.

## CONCLUSIONS AND OUTLOOK

We have described recent advances made during the past few years on the path toward bringing together the top-down whole cell biology approach and the bottom-up lipid mono- and supported planar bilayer physical chemistry approach for understanding molecular membrane biochemistry by using more realistic free-floating membrane systems on different length scales and characterizing them with emerging spectroscopic nonlinear scattering and imaging approaches. The molecular-level interfacial information about structure and hydration of more realistic free-floating nano-, micro- and macroscale membrane model systems in aqueous solution leads to several new directions of research either geared toward answering fundamental questions or obtaining more applied technological advancements.

**Fundamental Insights.** This Perspective shows a number of surprising findings from a more fundamental point of view. There is the structural difference between extended planar and nanoscopic interfaces ( $\sim 100$  nm sized), such as droplets and liposomes made out of the same chemicals as planar extended LMs or bilayers. This suggests that planar extended systems are limited as model systems for understanding real membranes in cells, and that length scale, curvature and confinement are more important parameters than previously thought. To obtain a further handle on this aspect, further experiments need to be performed, preferably in combination with modeling to determine which interactions change over what length scale.

The aspects of confinement/curvature and heterogeneity have not been previously considered in the molecular description of membranes. Since the experimental work described here shows they are important, and as it is also

shown that mean field models cannot anymore describe the electrostatics of droplet and liposome interfaces or the electrostatics of freestanding lipid membranes, it is necessary to expand theoretical modeling with sufficient atomistic detail to the length scale between  $\sim 10$  nm and  $\sim 10$   $\mu$ m. This could be explored in conjunction with experiments that probe for example the electrostatic or the hydration/hydrogen bond network structure on different length scales.

The presence of structural fluctuations in membrane hydration that gives rises to changes in the electrostatic energy on the order of 10 kT, are particularly striking and could prove to be significant game changers in our understanding of membrane or even liquid interface chemistry and physics. Since these fluctuations occur even in the liquid phase of partially charged membranes, they are likely to play a role in a wide variety of phenomena, ranging from simple ion–membrane interactions to protein membrane interactions, to intermembrane energy conversion. Future experiments should focus on understanding the origin of the membrane potential fluctuations and determining if they occur also in other phenomena (such as simple processes like ion–membrane interactions). As the neuroimaging experiments also demonstrate clear structural and temporal activity distributions, a connection might be made with ion channels as these are likely the key players in the movement of water and charges. Future experiments of interest would be to insert and activate ion channels in FLMs and to measure their influence on the water structure.

**Technological Advancement.** The recent technological developments described here have created tools to investigate molecular structure of lipid droplets and liposomes. Measurements of molecular conformation, tilt angles, chirality and interactions will lead to a better characterization of the interfacial chemistry of such systems. They can also bring new insights into the distribution of lipids and the coupling between domains and leaflets. The technology opens up new possibilities for the investigation of simple ion–membrane interactions, protein membrane interactions, enzyme activity and for example the working of ion channels and pores.

This will further the possibilities of developing and understanding the working of new drugs. The ability to measure membrane potentials either by scattering or by imaging brings about a wealth of possibilities for quantitative biology experiments. One example is the ability to measure and quantify membrane potentials and ion fluxes in living neurons. Such measurements can in the future lead to a better understanding of the electrostatic signaling between and within neurons, and eventually in tissue. Future advancements in optical technology can increase the temporal resolution so that also faster phenomena can be explored. Other cells that have membrane potential fluctuations such as muscle or cardiac cells can be investigated, which could be of interested in relation to the screening of drugs, or response of the cells or tissue to certain stimuli.

## AUTHOR INFORMATION

### Corresponding Author

\*sylvie.roke@epfl.ch

### ORCID

Halil I. Okur: 0000-0002-2492-1168

Sylvie Roke: 0000-0002-6062-7871

## Notes

The authors declare no competing financial interest.

## ACKNOWLEDGMENTS

This research has been supported by the Julia Jacobi Foundation and the Swiss National Foundation (grant numbers 200021\_146884 and 200021\_140472), European Research Council (grant numbers 240556 and 616305).

## REFERENCES

- (1) Grecco, H. E.; Schmick, M.; Bastiaens, P. I. H. Signaling from the living plasma membrane. *Cell* **2011**, *144* (6), 897–909.
- (2) Sunshine, H.; Iruela-Arispe, M. L. Membrane lipids and cell signaling. *Curr. Opin. Lipidol.* **2017**, *28* (5), 408–413.
- (3) Kühlbrandt, W. Structure and function of mitochondrial membrane protein complexes. *BMC Biol.* **2015**, *13* (1), 89.
- (4) Rathore, S.; Berndtsson, J.; Marin-Buera, L.; Conrad, J.; Carroni, M.; Brzezinski, P.; Ott, M. Cryo-EM structure of the yeast respiratory supercomplex. *Nat. Struct. Mol. Biol.* **2019**, *26* (1), 50–57.
- (5) Tauchi-Sato, K.; Ozeki, S.; Houjou, T.; Taguchi, R.; Fujimoto, T. The Surface of lipid droplets is a phospholipid monolayer with a unique fatty acid composition. *J. Biol. Chem.* **2002**, *277* (46), 44507–44512.
- (6) Walther, T. C.; Farese, R. V., Jr. Lipid droplets and Cellular Lipid Metabolism. *Annu. Rev. Biochem.* **2012**, *81* (1), 687–714.
- (7) Thiam, A. R.; Farese Jr, R. V.; Walther, T. C. The biophysics and cell biology of lipid droplets. *Nat. Rev. Mol. Cell Biol.* **2013**, *14* (12), 775–786.
- (8) Bartz, R.; Li, W.-H.; Venables, B.; Zehmer, J. K.; Roth, M. R.; Welti, R.; Anderson, R. G. W.; Liu, P.; Chapman, K. D. Lipidomics reveals that adiposomes store ether lipids and mediate phospholipid traffic. *J. Lipid Res.* **2007**, *48* (4), 837–847.
- (9) Singer, S. J.; Nicolson, G. L. The fluid mosaic model of the structure of cell membranes. *Science* **1972**, *175* (4023), 720.
- (10) Simons, K.; Vaz, W. L. C. Model systems, lipid rafts, and cell membranes. *Annu. Rev. Biophys. Biomol. Struct.* **2004**, *33*, 269–295.
- (11) van Meer, G.; de Kroon, A. I. P. M. Lipid map of the mammalian cell. *J. Cell Sci.* **2011**, *124* (1), 5–8.
- (12) Marsh, D. *Handbook of Lipid Bilayers*; CRC Press: Boca Raton, 2013.
- (13) Lutgebaucks, C.; Gonella, G.; Roke, S. Optical label-free and model-free probe of the surface potential of nanoscale and microscopic objects in aqueous solution. *Phys. Rev. B: Condens. Matter Mater. Phys.* **2016**, *94* (19), DOI: 10.1103/PhysRevB.94.195410.
- (14) Lütgebaucks, C.; Macias-Romero, C.; Roke, S. Characterization of the interface of binary mixed DOPC:DOPS liposomes in water: The impact of charge condensation. *J. Chem. Phys.* **2017**, *146* (4), 044701.
- (15) Tarun, O. B.; Hanneschläger, C.; Pohl, P.; Roke, S. Label-free and charge-sensitive dynamic imaging of lipid membrane hydration on millisecond time scales. *Proc. Natl. Acad. Sci. U. S. A.* **2018**, *115* (16), 4081–4086.
- (16) Cevc, G. Membrane electrostatics. *Biochimica et Biophysica Acta (BBA). Biochim. Biophys. Acta, Rev. Biomembr.* **1990**, *1031* (3), 311–382.
- (17) McLaughlin, S.; Murray, D. Plasma membrane phosphoinositide organization by protein electrostatics. *Nature* **2005**, *438* (7068), 605–611.
- (18) Jonsson, M. P.; Jönsson, P.; Dahlin, A. B.; Höök, F. Supported lipid bilayer formation and lipid-membrane-mediated biorecognition reactions studied with a new nanoplasmonic sensor template. *Nano Lett.* **2007**, *7* (11), 3462–3468.
- (19) Nguyen, T. T.; Conboy, J. C. High-Throughput screening of drug lipid membrane interactions via counter-propagating second harmonic generation imaging. *Anal. Chem.* **2011**, *83*, 5979–5988.
- (20) Feigenson, G. W. Phase Boundaries and Biological Membranes. *Annu. Rev. Biophys. Biomol. Struct.* **2007**, *36* (1), 63–77.

- (21) van Meer, G.; de Kroon, A. I. P. M. Lipid map of the mammalian cell. *J. Cell Sci.* **2011**, *124* (1), 5–8.
- (22) Cicuta, P.; Keller, S. L.; Veatch, S. L. Diffusion of Liquid Domains in Lipid Bilayer Membranes. *J. Phys. Chem. B* **2007**, *111* (13), 3328–3331.
- (23) Tarun, O. B.; Eremchev, M. Y.; Roke, S. Interaction of oil and lipids in freestanding lipid bilayer membranes studied with label-free high-throughput wide-field second-harmonic microscopy. *Langmuir* **2018**, *34* (38), 11305–11310.
- (24) Veatch, S. L.; Keller, S. L. Seeing spots: complex phase behavior in simple membranes. *Biochim. Biophys. Acta, Mol. Cell Res.* **2005**, *1746*, 172–185.
- (25) Marsh, D. Lateral Pressure Profile, Spontaneous Curvature Frustration, and the Incorporation and Conformation of Proteins in Membranes. *Biophys. J.* **2007**, *93* (11), 3884–3899.
- (26) Jarsch, I. K.; Daste, F.; Gallop, J. L. Membrane curvature in cell biology: An integration of molecular mechanisms. *J. Cell Biol.* **2016**, *214* (4), 375–387.
- (27) Groves, J. T. Bending Mechanics and Molecular Organization in Biological Membranes. *Annu. Rev. Phys. Chem.* **2007**, *58* (1), 697–717.
- (28) Eggeling, C.; Ringemann, C.; Medda, R.; Schwarzmann, G.; Sandhoff, K.; Polyakova, S.; Belov, V. N.; Hein, B.; von Middendorff, C.; Schonle, A.; Hell, S. W. Direct observation of the nanoscale dynamics of membrane lipids in a living cell. *Nature* **2009**, *457* (7233), 1159–1162.
- (29) de Wit, G.; Daniai, J. S. H.; Kukura, P.; Wallace, M. I. Dynamic label-free imaging of lipid nanodomains. *Proc. Natl. Acad. Sci. U. S. A.* **2015**, *112* (40), 12299–12303.
- (30) Korklach, J.; Schwill, P.; Webb, W. W.; Feigenson, G. W. Characterization of lipid bilayer phases by confocal microscopy and fluorescence correlation spectroscopy. *Proc. Natl. Acad. Sci. U. S. A.* **1999**, *96* (15), 8461–8466.
- (31) Kress, A.; Wang, X.; Ranchon, H.; Savatier, J.; Rigneault, H.; Ferrand, P.; Brasselet, S. Mapping the local organization of cell membranes using excitation-polarization-resolved confocal fluorescence microscopy. *Biophys. J.* **2013**, *105* (1), 127–136.
- (32) Shtengel, G.; Galbraith, J. A.; Galbraith, C. G.; Lippincott-Schwartz, J.; Gillette, J. M.; Manley, S.; Sougrat, R.; Waterman, C. M.; Kanchanawong, P.; Davidson, M. W.; Fetter, R. D.; Hess, H. F. Interferometric fluorescent super-resolution microscopy resolves 3D cellular ultrastructure. *Proc. Natl. Acad. Sci. U. S. A.* **2009**, *106* (9), 3125–3130.
- (33) Nuriya, M.; Yasui, M. Membrane potential dynamics of axons in cultured hippocampal neurons probed by second-harmonic-generation imaging. *J. Biomed. Opt.* **2010**, *15* (2), 020503.
- (34) Gurau, M.; Kim, G.; Lim, S. M.; Fleisher, H. C.; Cremer, P. S. Water structure and dynamics at fatty acid monolayer interfaces with divalent metal ions. *Biophys. J.* **2003**, *84* (2), 49a–49a.
- (35) Roke, S.; Schins, J.; Müller, M.; Bonn, M. Vibrational spectroscopic investigation of the phase diagram of a biomimetic lipid monolayer. *Phys. Rev. Lett.* **2003**, *90* (12), 128101–128101.
- (36) Ma, G.; Allen, H. C. Real-time investigation of lung surfactant respreading with surface vibrational spectroscopy. *Langmuir* **2006**, *22* (26), 11267–11274.
- (37) Ma, G.; Allen, H. C. DPPC Langmuir monolayer at the air-water interface: probing the tail and head groups by vibrational sum frequency generation spectroscopy. *Langmuir* **2006**, *22* (12), 5341–5349.
- (38) Mondal, J. A.; Nihonyanagi, S.; Yamaguchi, S.; Tahara, T. Three distinct water structures at a zwitterionic lipid/water interface revealed by heterodyne-detected vibrational sum frequency generation. *J. Am. Chem. Soc.* **2012**, *134* (18), 7842–7850.
- (39) Cremer, P. S.; Boxer, S. G. Formation and Spreading of Lipid Bilayers on Planar Glass Supports. *J. Phys. Chem. B* **1999**, *103* (13), 2554–2559.
- (40) Castellana, E. T.; Cremer, P. S. Solid supported lipid bilayers: From biophysical studies to sensor design. *Surf. Sci. Rep.* **2006**, *61* (10), 429–444.
- (41) Richter, R. P.; Berat, R.; Brisson, A. R. Formation of solid-supported lipid bilayers: An integrated view. *Langmuir* **2006**, *22* (8), 3497–3505.
- (42) Liu, J.; Conboy, J. C. Direct measurement of the transbilayer movement of phospholipids by sum-frequency vibrational spectroscopy. *J. Am. Chem. Soc.* **2004**, *126*, 8376–8377.
- (43) Ries, R. S.; Choi, H.; Blunck, R.; Bezanilla, F.; Heath, J. R. Black lipid membranes: visualizing the structure, dynamics, and substrate dependence of membranes. *J. Phys. Chem. B* **2004**, *108* (41), 16040–16049.
- (44) Chen, X. Y.; Wang, J.; Kristalyn, C. B.; Chen, Z. Real-time structural investigation of a lipid bilayer during its interaction with melittin using sum frequency generation vibrational spectroscopy. *Biophys. J.* **2007**, *93* (3), 866–875.
- (45) Casillas-Ituarte, N. N.; Chen, X.; Castada, H.; Allen, H. C. Na<sup>+</sup> and Ca<sup>2+</sup> effect on the hydration and orientation of the phosphate group of DPPC at air–water and air–hydrated silica interfaces. *J. Phys. Chem. B* **2010**, *114* (29), 9485–9495.
- (46) Chen, X.; Hua, W.; Huang, Z.; Allen, H. C. Interfacial water structure associated with phospholipid membranes studied by phase-sensitive vibrational sum frequency generation spectroscopy. *J. Am. Chem. Soc.* **2010**, *132*, 11336–11342.
- (47) Liljebblad, J. D. F.; Bulone, V.; Tyrode, E.; Rutland, M. W.; Johnson, C. M. Phospholipid monolayers probed by vibrational sum frequency spectroscopy: instability of unsaturated phospholipids. *Biophys. J.* **2010**, *98* (10), L50–L52.
- (48) Liu, B.; Lee, H. J.; Zhang, D.; Liao, C.-S.; Ji, N.; Xia, Y.; Cheng, J.-X. Label-free spectroscopic detection of membrane potential using stimulated Raman scattering. *Appl. Phys. Lett.* **2015**, *106* (17), 173704.
- (49) Geiger, F. M. Second harmonic generation, sum frequency generation, and  $\chi(3)$ : dissecting environmental interfaces with a nonlinear optical swiss army knife. *Annu. Rev. Phys. Chem.* **2009**, *60* (1), 61–83.
- (50) Roke, S.; Gonella, G. Nonlinear light scattering and spectroscopy of particles and droplets in liquids. *Annu. Rev. Phys. Chem.* **2012**, *63*, 353–378.
- (51) Gonella, G.; Lütgebaucks, C.; de Beer, A. G. F.; Roke, S. Second harmonic and sum-frequency generation from aqueous interfaces is modulated by interference. *J. Phys. Chem. C* **2016**, *120* (17), 9165–9173.
- (52) Darlington, A. M.; Jarisz, T. A.; DeWalt-Kerian, E. L.; Roy, S.; Kim, S.; Azam, M. S.; Hore, D. K.; Gibbs, J. M. Separating the pH-dependent behavior of water in the Stern and diffuse layers with varying salt concentration. *J. Phys. Chem. C* **2017**, *121* (37), 20229–20241.
- (53) Chen, Y.; Jena, K. C.; Lütgebaucks, C.; Okur, H. I.; Roke, S. Three dimensional nano “Langmuir trough” for lipid studies. *Nano Lett.* **2015**, *15* (8), 5558–5563.
- (54) Singh, P. C.; Inoue, K.; Nihonyanagi, S.; Yamaguchi, S.; Tahara, T. Femtosecond hydrogen bond dynamics of bulk-like and bound water at positively and negatively charged lipid interfaces revealed by 2D HD-VSFG spectroscopy. *Angew. Chem., Int. Ed.* **2016**, *55* (36), 10621–10625.
- (55) Pullanchery, S.; Yang, T.; Cremer, P. S. Introduction of positive charges into zwitterionic phospholipid monolayers disrupts water structure whereas negative charges enhances it. *J. Phys. Chem. B* **2018**, *122* (51), 12260–12270.
- (56) Vezočnik, V.; Hodnik, V.; Sitar, S.; Okur, H. I.; Tušek-Žnidarič, M.; Lütgebaucks, C.; Sepčić, K.; Kogej, K.; Roke, S.; Žagar, E.; Maček, P. Kinetically stable triglyceride-based nanodroplets and their interactions with lipid-specific proteins. *Langmuir* **2018**, *34*, 8983.
- (57) Chen, Y.; Okur, H. I.; Lütgebaucks, C.; Roke, S. Zwitterionic and charged lipids form remarkably different structures on nanoscale oil droplets in aqueous solution. *Langmuir* **2018**, *34* (3), 1042–1050.
- (58) Okur, H. I.; Chen, Y.; Smolentsev, N.; Zdrali, E.; Roke, S. Interfacial structure and hydration of 3D lipid monolayers in aqueous solution. *J. Phys. Chem. B* **2017**, *121* (13), 2808–2813.

- (59) Smolentsev, N.; Lütgebaucks, C.; Okur, H. I.; de Beer, A. G. F.; Roke, S. Intermolecular headgroup interaction and hydration as driving forces for lipid transmembrane asymmetry. *J. Am. Chem. Soc.* **2016**, *138* (12), 4053–4060.
- (60) Gonella, G.; Lütgebaucks, C.; de Beer, A. G. F.; Roke, S. Second harmonic and sum-frequency generation from aqueous interfaces is modulated by interference. *J. Phys. Chem. C* **2016**, *120* (17), 9165–9173.
- (61) Adams, E. M.; Casper, C. B.; Allen, H. C. Effect of cation enrichment on dipalmitoylphosphatidylcholine (DPPC) monolayers at the air-water interface. *J. Colloid Interface Sci.* **2016**, *478*, 353–364.
- (62) Melcrová, A.; Pokorna, S.; Pullanchery, S.; Kohagen, M.; Jurkiewicz, P.; Hof, M.; Jungwirth, P.; Cremer, P. S.; Cwiklik, L. The complex nature of calcium cation interactions with phospholipid bilayers. *Sci. Rep.* **2016**, *6*, 38035.
- (63) Watry, M. R.; Tarbuck, T. L.; Richmond, G. L. Vibrational sum-frequency studies of a series of phospholipid monolayers and the associated water structure at the vapor/water interface. *J. Phys. Chem. B* **2003**, *107* (2), 512–518.
- (64) Walker, R. A.; Conboy, J. C.; Richmond, G. L. Molecular structure and ordering of phospholipids at a liquid-liquid interface. *Langmuir* **1997**, *13* (12), 3070–3073.
- (65) Okur, H. I.; Hladilkova, J.; Rembert, K. B.; Cho, Y.; Heyda, J.; Dzubilla, J.; Cremer, P. S.; Jungwirth, P. Beyond the Hofmeister series: ion-specific effects on proteins and their biological functions. *J. Phys. Chem. B* **2017**, *121* (9), 1997–2014.
- (66) Yan, E. C. Y.; Fu, L.; Wang, Z.; Liu, W. Biological macromolecules at interfaces probed by chiral vibrational sum frequency generation spectroscopy. *Chem. Rev.* **2014**, *114* (17), 8471–8498.
- (67) Troiano, J. M.; Olenick, L. L.; Kuech, T. R.; Melby, E. S.; Hu, D.; Lohse, S. E.; Mensch, A. C.; Dogangun, M.; Vartanian, A. M.; Torelli, M. D.; Ehimiaghe, E.; Walter, S. R.; Fu, L.; Anderton, C. R.; Zhu, Z.; Wang, H.; Orr, G.; Murphy, C. J.; Hamers, R. J.; Pedersen, J. A.; Geiger, F. M. Direct probes of 4 nm diameter gold nanoparticles interacting with supported lipid bilayers. *J. Phys. Chem. C* **2015**, *119* (1), 534–546.
- (68) Kocsis, I.; Sorci, M.; Vanselous, H.; Murail, S.; Sanders, S. E.; Licsandru, E.; Legrand, Y. M.; van der Lee, A.; Baaden, M.; Petersen, P. B.; Belfort, G.; Barboiu, M. Oriented chiral water wires in artificial transmembrane channels. *Sci. Adv.* **2018**, *4* (3), eaao5603.
- (69) Dreier, L. B.; Nagata, Y.; Lutz, H.; Gonella, G.; Hunger, J.; Backus, E. H. G.; Bonn, M. Saturation of charge-induced water alignment at model membrane surfaces. *Sci. Adv.* **2018**, *4* (3), eaap7415.
- (70) Adams, E. M.; Verreault, D.; Jayarathne, T.; Cochran, R. E.; Stone, E. A.; Allen, H. C. Surface organization of a DPPC monolayer on concentrated SrCl<sub>2</sub> and ZnCl<sub>2</sub> solutions. *Phys. Chem. Chem. Phys.* **2016**, *18* (47), 32345–32357.
- (71) Cong, X.; Poyton, M. F.; Baxter, A. J.; Pullanchery, S.; Cremer, P. S. Unquenchable Surface Potential Dramatically Enhances Cu<sup>2+</sup> Binding to Phosphatidylserine Lipids. *J. Am. Chem. Soc.* **2015**, *137* (24), 7785–7792.
- (72) Troiano, J. M.; McGeachy, A. C.; Olenick, L. L.; Fang, D.; Liang, D.; Hong, J.; Kuech, T. R.; Caudill, E. R.; Pedersen, J. A.; Cui, Q.; Geiger, F. M. Quantifying the electrostatics of polycation–lipid bilayer interactions. *J. Am. Chem. Soc.* **2017**, *139* (16), 5808–5816.
- (73) Gurtovenko, A. A.; Vattulainen, I. Effect of NaCl and KCl on phosphatidylcholine and phosphatidylethanolamine lipid membranes: insight from atomic-scale simulations for understanding salt-induced effects in the plasma membrane. *J. Phys. Chem. B* **2008**, *112* (7), 1953–1962.
- (74) Lindahl, E.; Sansom, M. S. P. Membrane proteins: molecular dynamics simulations. *Curr. Opin. Struct. Biol.* **2008**, *18* (4), 425–431.
- (75) Ingólfsson, H. I.; Arnarez, C.; Periole, X.; Marrink, S. J. Computational ‘microscopy’ of cellular membranes. *J. Cell Sci.* **2016**, *129* (2), 257–268.
- (76) Maffeo, C.; Bhattacharya, S.; Yoo, J.; Wells, D.; Aksimentiev, A. Modeling and simulation of ion channels. *Chem. Rev.* **2012**, *112* (12), 6250–6284.
- (77) Shen, Y.-X.; Song, W.; Barden, D. R.; Ren, T.; Lang, C.; Feroz, H.; Henderson, C. B.; Saboe, P. O.; Tsai, D.; Yan, H.; Butler, P. J.; Bazan, G. C.; Phillip, W. A.; Hickey, R. J.; Cremer, P. S.; Vashisth, H.; Kumar, M. Achieving high permeability and enhanced selectivity for Angstrom-scale separations using artificial water channel membranes. *Nat. Commun.* **2018**, *9* (1), 2294.
- (78) Stokes, G. Y.; Gibbs-Davis, J. M.; Boman, F. C.; Stepp, B. R.; Condie, A. G.; Nguyen, S. T.; Geiger, F. M. Making “Sense” of DNA. *J. Am. Chem. Soc.* **2007**, *129* (24), 7492–7493.
- (79) McDermott, M. L.; Vanselous, H.; Corcelli, S. A.; Petersen, P. B. DNA’s chiral spine of hydration. *ACS Cent. Sci.* **2017**, *3* (7), 708–714.
- (80) Pandey, R.; Usui, K.; Livingstone, R. A.; Fischer, S. A.; Pfaendtner, J.; Backus, E. H. G.; Nagata, Y.; Fröhlich-Nowoisky, J.; Schmäser, L.; Mauri, S.; Scheel, J. F.; Knopf, D. A.; Pöschl, U.; Bonn, M.; Weidner, T. Ice-nucleating bacteria control the order and dynamics of interfacial water. *Sci. Adv.* **2016**, *2* (4), e1501630.
- (81) Krieche, M. A.; Conboy, J. C. Imaging chirality with surface second harmonic generation microscopy. *J. Am. Chem. Soc.* **2005**, *127* (9), 2834–2835.
- (82) Peterson, M. D.; Hayes, P. L.; Martinez, I. S.; Cass, L. C.; Achtyl, J. L.; Weiss, E. A.; Geiger, F. M. Second harmonic generation imaging with a kHz amplifier. *Opt. Mater. Express* **2011**, *1* (1), S7–66.
- (83) Petersen, P. B.; Saykally, R. J. Probing the interfacial structure of aqueous electrolytes with femtosecond second harmonic generation spectroscopy. *J. Phys. Chem. B* **2006**, *110* (29), 14060–14073.
- (84) Macias-Romero, C.; Didier, M. E. P.; Jourdain, P.; Marquet, P.; Magistretti, P.; Tarun, O. B.; Zubkovs, V.; Radenovic, A.; Roke, S. High throughput second harmonic imaging for label-free biological applications. *Opt. Express* **2014**, *22* (25), 31102–12.
- (85) Flörsheimer, M.; Brillert, C.; Fuchs, H. Chemical imaging of interfaces by sum frequency microscopy. *Langmuir* **1999**, *15* (17), 5437–5439.
- (86) Cimat, K.; Baldelli, S. Sum frequency generation imaging microscopy of CO on platinum. *J. Am. Chem. Soc.* **2006**, *128* (50), 16016–16017.
- (87) Smith, K. A.; Conboy, J. C. A Simplified sum-frequency vibrational imaging setup used for imaging lipid bilayer arrays. *Anal. Chem.* **2012**, *84* (19), 8122–8126.
- (88) Raghunathan, V.; Han, Y.; Korth, O.; Ge, N.-H.; Potma, E. O. Rapid vibrational imaging with sum frequency generation microscopy. *Opt. Lett.* **2011**, *36* (19), 3891–3893.
- (89) Roke, S.; Roeterdink, W. G.; Wijnhoven, J. E. G. J.; Petukhov, A. V.; Kleyn, A. W.; Bonn, M. Vibrational sum frequency scattering from a sub-micron suspension. *Phys. Rev. Lett.* **2003**, *91*, 258302–258302.
- (90) Gomopoulos, N.; Lütgebaucks, C.; Sun, Q.; Macias-Romero, C.; Roke, S. Label-free second harmonic and hyper Rayleigh scattering with high efficiency. *Opt. Express* **2013**, *21*, 815.
- (91) de Aguiar, H. B.; Samson, J. S.; Roke, S. Probing nanoscopic droplet interfaces in aqueous solution with vibrational sum-frequency scattering: a study of the effects of path length, droplet density and pulse energy. *Chem. Phys. Lett.* **2011**, *512*, 76–80.
- (92) de Beer, A. G. F.; Campen, R. K.; Roke, S. Separating surface structure and surface charge with second-harmonic and sum-frequency scattering. *Phys. Rev. B: Condens. Matter Mater. Phys.* **2010**, *82*, 235431.
- (93) Jena, K. C.; Scheu, R.; Roke, S. Surface impurities are not responsible for the charge on the oil/water interface: a comment. *Angew. Chem., Int. Ed.* **2012**, *51* (52), 12938–12940.
- (94) de Aguiar, H. B.; de Beer, A. G. F.; Strader, M. L.; Roke, S. The interfacial tension of nanoscopic oil droplets in water is hardly affected by SDS surfactant. *J. Am. Chem. Soc.* **2010**, *132* (7), 2122–2123.

- (95) de Aguiar, H. B.; Strader, M. L.; de Beer, A. G. F.; Roke, S. Surface structure of SDS surfactant and oil at the oil-in-water droplet liquid/liquid interface: a manifestation of a non-equilibrium surface state. *J. Phys. Chem. B* **2011**, *115*, 2970–2978.
- (96) Vácha, R.; Rick, S. W.; Jungwirth, P.; de Beer, A. G. F.; de Aguiar, H. B.; Samson, J. S.; Roke, S. The orientation and charge of water at the hydrophobic oil droplet-water interface. *J. Am. Chem. Soc.* **2011**, *133*, 10204–10210.
- (97) Scheu, R.; Chen, Y.; de Aguiar, H. B.; Rankin, B. M.; Ben-Amotz, D.; Roke, S. Specific ion effects in amphiphile hydration and interface stabilization. *J. Am. Chem. Soc.* **2014**, *136* (5), 2040–2047.
- (98) Scheu, R.; Rankin, B. M.; Chen, Y.; Jena, K. C.; Ben-Amotz, D.; Roke, S. Charge asymmetry at aqueous hydrophobic interfaces and hydration shells. *Angew. Chem., Int. Ed.* **2014**, *53* (36), 9560–9563.
- (99) Smolentsev, N.; Smit, W. J.; Bakker, H. J.; Roke, S. The interfacial structure of water droplets in a hydrophobic liquid. *Nat. Commun.* **2017**, *8*, 15548.
- (100) de Aguiar, H. B.; de Beer, A. G. F.; Roke, S. The Presence of Ultralow Densities of Nanocrystallites in Amorphous Poly(lactic acid) Microspheres. *J. Phys. Chem. B* **2013**, *117*, 8906–8910.
- (101) Strader, M. L.; de Aguiar, H. B.; de Beer, A. G. F.; Roke, S. Label-free spectroscopic detection of vesicles in water using vibrational sum frequency scattering. *Soft Matter* **2011**, *7* (10), 4959–4963.
- (102) de Beer, A. G. F.; de Aguiar, H. B.; Nijsen, J. F. W.; Roke, S. Detection of buried microstructures by nonlinear light scattering spectroscopy. *Phys. Rev. Lett.* **2009**, *102* (9), 095502.
- (103) Johansson, P. K.; Koelsch, P. Vibrational sum-frequency scattering for detailed studies of collagen fibers in aqueous environments. *J. Am. Chem. Soc.* **2014**, *136* (39), 13598–13601.
- (104) Makarem, M.; Lee, C. M.; Sawada, D.; O'Neill, H. M.; Kim, S. H. Distinguishing surface versus bulk hydroxyl groups of cellulose nanocrystals using vibrational sum frequency generation spectroscopy. *J. Phys. Chem. Lett.* **2018**, *9* (1), 70–75.
- (105) Wang, H.; Yan, E. C. Y.; Borguet, E.; Eienthal, K. B. Second harmonic generation from the surface of centrosymmetric particles in bulk solution. *Chem. Phys. Lett.* **1996**, *259*, 15–20.
- (106) Eienthal, K. B. Second Harmonic Spectroscopy of Aqueous Nano- and Microparticle Interfaces. *Chem. Rev.* **2006**, *106* (4), 1462–1477.
- (107) Yan, E. C. Y.; Liu, Y.; Eienthal, K. B. New Method for Determination of Surface Potential of Microscopic Particles by Second Harmonic Generation. *J. Phys. Chem. B* **1998**, *102* (33), 6331–6336.
- (108) Liu, Y.; Yan, E. C. Y.; Eienthal, K. B. Effects of bilayer surface charge density on molecular adsorption and transport across liposome bilayers. *Biophys. J.* **2001**, *80*, 1004–1012.
- (109) Wilhelm, M. J.; Sheffield, J. B.; Sharifian Gh, M.; Wu, Y.; Spahr, C.; Gonella, G.; Xu, B.; Dai, H.-L. Gram's stain does not cross the bacterial cytoplasmic membrane. *ACS Chem. Biol.* **2015**, *10* (7), 1711–1717.
- (110) Sharifian Gh, M.; Wilhelm, M. J.; Dai, H.-L. Azithromycin-induced changes to bacterial membrane properties monitored in vitro by second-harmonic light scattering. *ACS Med. Chem. Lett.* **2018**, *9* (6), 569–574.
- (111) Shang, X.; Liu, Y.; Yan, E.; Eienthal, K. B. Effects of counterions on molecular transport across liposome bilayer: probed by second harmonic generation. *J. Phys. Chem. B* **2001**, *105* (51), 12816–12822.
- (112) Sharifian Gh, M.; Wilhelm, M. J.; Dai, H.-L. Label-Free optical method for quantifying molecular transport across cellular membranes in vitro. *J. Phys. Chem. Lett.* **2016**, *7* (17), 3406–3411.
- (113) Zdrali, E.; Chen, Y.; Okur, H. I.; Wilkins, D. M.; Roke, S. The molecular mechanism of nanodroplet stability. *ACS Nano* **2017**, *11* (12), 12111–12120.
- (114) Israelachvili, J. N. *Intermolecular and Surface Forces*; Academic Press: Oxford, 2011.
- (115) de Beer, A. G. F.; Roke, S. Nonlinear Mie theory for second-harmonic and sum-frequency scattering. *Phys. Rev. B: Condens. Matter Mater. Phys.* **2009**, *79* (15), 155420.
- (116) Anghel, V. N. P.; Kucerka, N.; Pencer, J.; Katsaras, J. Scattering from laterally heterogeneous vesicles. II. The form factor. *J. Appl. Crystallogr.* **2007**, *40* (3), 513–525.
- (117) Liu, Y.; Yan, E. C. Y.; Zhao, X.; Eienthal, K. B. Surface potential of charged liposomes determined by second harmonic generation. *Langmuir* **2001**, *17* (7), 2063–2066.
- (118) Casal, H. L.; Mantsch, H. H.; Paltauf, F.; Hauser, H. Infrared and <sup>31</sup>P-NMR studies of the effect of Li<sup>+</sup> and Ca<sup>2+</sup> on phosphatidylserines. *Biochim. Biophys. Acta, Lipids Lipid Metab.* **1987**, *919* (3), 275–286.
- (119) Hunter, R. J. *Foundations of Colloid Science*; Oxford University Press, 2001.
- (120) de Beer, A. G. F.; Campen, R. K.; Roke, S. Separating surface structure and surface charge with second-harmonic and sum-frequency scattering. *Phys. Rev. B: Condens. Matter Mater. Phys.* **2010**, *82* (23), 23541.
- (121) de Beer, A. G. F.; Roke, S. Obtaining molecular orientation from second harmonic and sum frequency scattering experiments in water: Angular distribution and polarization dependence. *J. Chem. Phys.* **2010**, *132* (23), 234702.
- (122) Lee, C. H. C.; Chang, R. K.; Bloembergen, N. Nonlinear electroreflectance in silicon and silver. *Phys. Rev. Lett.* **1967**, *18*, 167–170.
- (123) Yan, E. C. Y.; Liu, Y.; Eienthal, K. B. New method for determination of surface potential of microscopic particles by second harmonic generation. *J. Phys. Chem. B* **1998**, *102* (33), 6331–6336.
- (124) Evans, C. L.; Potma, E. O.; Puoris'haag, M.; Côté, D.; Lin, C. P.; Xie, X. S. Chemical imaging of tissue in vivo with video-rate coherent anti-Stokes Raman scattering microscopy. *Proc. Natl. Acad. Sci. U. S. A.* **2005**, *102* (46), 16807–16812.
- (125) Lucotte, B. M.; Powell, C.; Knutson, J. R.; Combs, C. A.; Malide, D.; Yu, Z.-X.; Knepper, M.; Patel, K. D.; Pielach, A.; Johnson, E.; Borysova, L.; Dora, K. A.; Balaban, R. S. Direct visualization of the arterial wall water permeability barrier using CARS microscopy. *Proc. Natl. Acad. Sci. U. S. A.* **2017**, *114* (18), 4805–4810.
- (126) Chen, Y.; Jena, K. C.; Roke, S. From hydrophobic to hydrophilic: the structure and density of the hexadecane droplet/alkanol/water interface. *J. Phys. Chem. C* **2015**, *119* (31), 17725–17734.
- (127) Zdrali, E.; Baer, M. D.; Okur, H. I.; Mundy, C. J.; Roke, S. The diverse nature of ion speciation at the nanoscale hydrophobic/water interface. *J. Phys. Chem. B* **2019**, *123* (10), 2414–2423.
- (128) Jackson, J. D. *Classical Electrodynamics*; John Wiley & Sons: New York, 1998.
- (129) Oshima, H. *Theory of Colloid and Interfacial phenomena*; Academic Press: Oxford, 2006.
- (130) Nan, X.; Cheng, J.-X.; Xie, X. S. Vibrational imaging of lipid droplets in live fibroblast cells with coherent anti-Stokes Raman scattering microscopy. *J. Lipid Res.* **2003**, *44* (11), 2202–2208.
- (131) Potma, E. O.; de Boeij, W. P.; van Haastert, P. J. M.; Wiersma, D. A. Real-time visualization of intracellular hydrodynamics in single living cells. *Proc. Natl. Acad. Sci. U. S. A.* **2001**, *98* (4), 1577–1582.
- (132) Cheng, J.-X.; Pautot, S.; Weitz, D. A.; Xie, X. S. Ordering of water molecules between phospholipid bilayers visualized by coherent anti-Stokes Raman scattering microscopy. *Proc. Natl. Acad. Sci. U. S. A.* **2003**, *100* (17), 9826–9830.
- (133) Macias-Romero, C.; Nahalka, I.; Okur, H. I.; Roke, S. Optical imaging of surface chemistry and dynamics in confinement. *Science* **2017**, *357* (6353), 784.
- (134) Montal, M.; Mueller, P. Formation of bimolecular membranes from lipid monolayers and a study of their electrical properties. *Proc. Natl. Acad. Sci. U. S. A.* **1972**, *69* (12), 3561–3566.
- (135) Gutschmann, T.; Heimburg, T.; Keyser, U.; Mahendran, K. R.; Winterhalter, M. Protein reconstitution into freestanding planar lipid membranes for electrophysiological characterization. *Nat. Protoc.* **2015**, *10*, 188.

- (136) Alvarez, O.; Latorre, R. Voltage-dependent capacitance in lipid bilayers made from monolayers. *Biophys. J.* **1978**, *21* (1), 1–17.
- (137) White, S. H.; Petersen, D. C.; Simon, S.; Yafuso, M. Formation of planar bilayer membranes from lipid monolayers. a critique. *Biophys. J.* **1976**, *16* (5), 481–489.
- (138) Melikov, K. C.; Frolov, V. A.; Shcherbakov, A.; Samsonov, A. V.; Chizmadzhev, Y. A.; Chernomordik, L. V. Voltage-induced nonconductive pre-pores and metastable single pores in unmodified planar lipid bilayer. *Biophys. J.* **2001**, *80* (4), 1829–1836.
- (139) Heimburg, T. Lipid ion channels. *Biophys. Chem.* **2010**, *150* (1), 2–22.
- (140) Neher, E.; Sakmann, B. Single-channel currents recorded from membrane of denervated frog muscle fibres. *Nature* **1976**, *260* (5554), 799–802.
- (141) Wunderlich, B.; Leirer, C.; Idzko, A. L.; Keyser, U. F.; Wixforth, A.; Myles, V. M.; Heimburg, T.; Schneider, M. F. Phase-State dependent current fluctuations in pure lipid membranes. *Biophys. J.* **2009**, *96* (11), 4592–4597.
- (142) Smetters, D.; Majewska, A.; Yuste, R. Detecting action potentials in neuronal populations with calcium imaging. *Methods* **1999**, *18* (2), 215–221.
- (143) Nguyen, J. P.; Shipley, F. B.; Linder, A. N.; Plummer, G. S.; Liu, M.; Setru, S. U.; Shaevitz, J. W.; Leifer, A. M. Whole-brain calcium imaging with cellular resolution in freely behaving *Caenorhabditis elegans*. *Proc. Natl. Acad. Sci. U. S. A.* **2016**, *113* (8), E1074–E1081.
- (144) Packer, A. M.; Roska, B.; Häusser, M. Targeting neurons and photons for optogenetics. *Nat. Neurosci.* **2013**, *16* (7), 805–815.
- (145) Knöpfel, T.; Diez-García, J.; Akemann, W. Optical probing of neuronal circuit dynamics: genetically encoded versus classical fluorescent sensors. *Trends Neurosci.* **2006**, *29* (3), 160–166.
- (146) Didier, M. E. P.; Tarun, O. B.; Jourdain, P.; Magistretti, P.; Roke, S. Membrane water for probing neuronal membrane potentials and ionic fluxes at the single cell level. *Nat. Commun.* **2018**, *9* (1), 5287.